University of Pennsylvania
ScholarlyCommons

Departmental Papers (MEAM)

Department of Mechanical Engineering & Applied Mechanics

6-8-2005

Magnetohydrodynamic flow of RedOx electrolyte

Shizhi Qian
University of Pennsylvania

Haim H. Bau
University of Pennsylvania, bau@seas.upenn.edu

Copyright (2005) American Institute of Physics. This article may be downloaded for personal use only. Any other use requires prior permission of the author and the American Institute of Physics. Reprinted in *Physics of Fluids*, Volume 17, Article 067105, 12 pages.
Publisher URL: http://dx.doi.org/10.1063/1.1933131

This paper is posted at ScholarlyCommons. http://repository.upenn.edu/meam_papers/107
For more information, please contact repository@pobox.upenn.edu.

HTML ABSTRACT + LINKS

Magnetohydrodynamic flow of RedOx electrolyte

Shizhi Qian and Haim H. Bau[a)]
Mechanical Engineering and Applied Mechanics, University of Pennsylvania, Philadelphia, Pennsylvania 19104-6315

(Received 27 January 2005; accepted 26 April 2005; published online 8 June 2005)

Magnetohydrodynamic (MHD) flow of a RedOx electrolyte in a straight conduit is investigated theoretically. Inert electrodes are deposited along segments of the opposing walls of a straight conduit that is filled with a RedOx electrolyte solution. The conduit is positioned in a uniform magnetic field. When a potential difference is applied across the opposing electrodes, the resulting current interacts with the magnetic field to induce Lorentz forces. The species' mass transport and the momentum equation are coupled and must be solved simultaneously. We compute the various species' concentration distributions, the current flux distribution, and the liquid's motion in the absence and presence of pressure gradients. The pressure gradients may either assist or oppose the MHD flow. At low potential differences, the current and the induced MHD flow increase nearly linearly as the potential difference increases. When the potential difference exceeds a certain critical value, the current and the flow rate saturate. We demonstrate that it is advantageous to use multiple electrode pairs with dielectric gaps between adjacent electrodes rather than a single electrode pair with an equivalent length. Finally, MHD flow with RedOx solution in the presence of abundant supporting electrolyte under limiting current conditions is analyzed using boundary layer theory. The approximate analytical solutions for the ions' concentrations and the current agree well with the numerical solutions. © *2005 American Institute of Physics*. [DOI: 10.1063/1.1933131]

I. INTRODUCTION

In recent years, there has been a growing interest in developing minute systems for biodetection, biotechnology, chemical reactors, electronic cooling, and medical, pharmaceutical, and environmental monitoring. In many of these applications, it is necessary to propel fluids from one part of the device to another, control fluid motion, stir, and separate fluids. In microdevices, these tasks are far from trivial. Magnetohydrodynamics (MHD) offers an elegant, inexpensive, flexible, customizable means of performing some of these functions.

The application of electromagnetic forces to pump, confine, and control fluids is by no means new, however, MHD has been mostly thought of in the context of highly conducting fluids such as liquid metals and ionized gases.[1,2] Recently, though, Jang and Lee,[3] Lemoff and Lee,[4] Bau,[5] and Zhong, Yi, and Bau[6] constructed MHD micropumps with silicon and ceramic substrates and demonstrated that these pumps are able to move liquids around in small conduits. Bau and co-workers[7–9] demonstrated the feasibility of using MHD forces to control fluid flow in microfluidic networks. By judicious application of potential differences across electrode pairs, one can direct the liquid to flow along any desired path without a need for valves and pumps. West *et al.*[10] fabricated a MHD continuous flow microreactor with three thermal zones in an attempt to facilitate the thermocycling needed for DNA amplification. Eijkel *et al.*[11] proposed a circular, open tubular chromatographic system based on the circular flow motion induced by MHD. Indeed, MHD propulsion is one of the few methods that allow pumping of liquids along a closed loop, thereby forming a conduit with an "infinite length."

In addition to pumping, MHD can facilitate stirring. West *et al.*[12] and Gleeson *et al.*[13] constructed and tested a toriodal MHD stirrer that takes advantage of Taylor dispersion[14] to increase the surface area between two interacting fluids. Alternatively, one can pattern electrodes of various shapes to induce electric fields in different directions. The interaction of such electric fields with the magnetic field induces secondary flows that may benefit stirring and mixing.[7] Although these secondary flows significantly enhance the mixing process, they are still laminar and the mixing is poor. One can do better, however. By periodically or aperiodically alternating among two or more different flow patterns, one can introduce (Lagrangian) chaotic advection.[15–18]

Although MHD technology has significant promise, it is not completely problem-free. Some of the issues of concern are potential bubble formation, electrode corrosion, and the depletion of electrolyte during operation. RedOx electrolytes that undergo reversible electrochemical reactions at the electrodes' surfaces eliminate many of these problems while facilitating relatively high current fluxes at low potential differences. Examples of such RedOx pairs are $FeCl_2/FeCl_3$ and potassium ferrocyanide $(K_4[Fe(CN)_6])$/potassium ferricyanide $(K_3[Fe(CN)_6])$ operating with inert (i.e., platinum) electrodes. In this paper, we will study the performance of a MHD pump operating with the RedOx pair $FeCl_3/FeCl_2$.

In all the papers cited above, the electrolyte was treated as an Ohmic conductor. Unlike in liquid metals,[2] the intensity of the electric current in electrolyte solutions depends

[a)]Author to whom correspondence should be addressed. Electronic mail: bau@seas.upenn.edu

 © 2005 American Institute of Physics

Downloaded 18 Oct 2007 to 158.130.69.60. Redistribution subject to AIP license or copyright, see http://pof.aip.org/pof/copyright.jsp

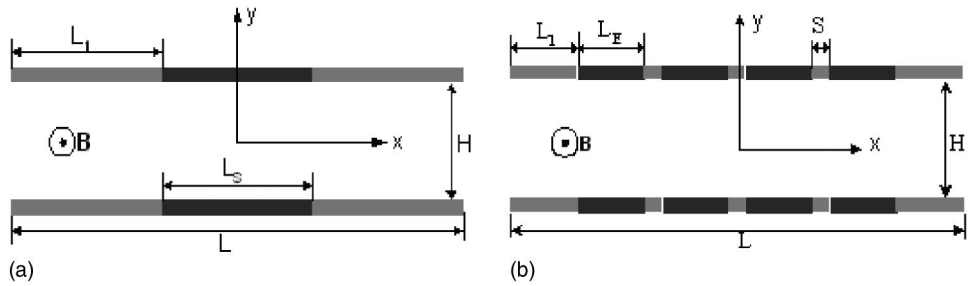

FIG. 1. A cross section of a straight conduit equipped with two long electrodes (a) and a number of short electrodes (b) positioned along opposing walls. The conduit is filled with RedOx electrolyte solution and subjected to a uniform magnetic field of intensity **B**. A potential difference ΔV is imposed across the electrodes that are facing each other.

strongly on the mass transfer. Hence, in this paper, we take a more rigorous approach and account for the effect of convection on the transport of ions in the electrolyte solution. In other words, we solve the conjugate problem in which the momentum and advection equations are coupled.

Although this paper focuses on microfluidic systems, the work presented here is also related to various electrochemical processes ranging from electroplating to fuel cells in which mass transfer and surface morphology can be controlled with external magnetic fields.[19] Electrochemical processes with magnetically assisted mass transfer have been dubbed magnetoelectrolysis.[20] Most of the prior works were experimental or consisted of order of magnitude estimates.[21–23] For example, when the gap between the electrodes is narrow, the flow is fully developed, and the Lorentz force balances the viscous forces, the limiting current is proportional to $B^{1/2}C_0^{3/2}$. When the gap between the electrodes is wide,[23,24] the flow consists of developing boundary layers, and the Lorentz force is balanced with inertial forces, the limiting current is proportional to $B^{1/3}C_0^{4/3}$. In the above, B is the magnetic field intensity and C_0 is the bulk concentration of the RedOx active species. These asymptotic relationships are consistent with experimental data.

Boum and Alemany[25] solved numerically the MHD flow of an electrolyte solution between two parallel electrodes in the presence of abundant supporting electrolyte and fast electrochemical reactions. These conditions allowed them to assume that the electric conductivity is uniform throughout the solution, to introduce an effective electric potential, and to ignore the electrode kinetics.

In this paper, we do not make the approximations mentioned above. We solve numerically the concentration, current, and flow distributions in flow driven by both pressure and Lorentz forces accounting for the electrochemical reactions at the electrode surfaces. The calculations are performed for sublimiting current conditions. We also derive a boundary layer theory under limiting current conditions that allows us to calculate the concentration and velocity fields with a relatively simple analytic formula without any adjustable parameters.

The paper is organized as follows. Section II introduces the mathematical model for the conjugate problem of MHD flow and ion transport. Section III describes the code validation by comparing our numerical predictions with a few special cases reported in the literature. Section IV provides the ions' concentration distributions and the flow field as functions of the external pressure gradient and the induced Lorentz force in the absence of supporting electrolyte. Section V provides an approximate boundary layer-based analysis of MHD flow with RedOx electrolyte in the presence of abundant supporting electrolyte under limiting current conditions. The approximate, analytical solutions are compared and favorably agree with the results of the numerical simulations. Section VI concludes the paper.

II. MATHEMATICAL MODEL

In this section, we introduce a mathematical model to describe the transport of ions in the solution. This model accounts for the oxidation and reduction reactions at the electrodes' surfaces and the convection induced by both the Lorentz force and the external pressure gradient. The device consists of a planar conduit of length L with a rectangular cross section of width W and height H. We use a Cartesian coordinate system x, y, and z with its origin at the conduit's center. The coordinates x, y, and z are aligned, respectively, along the conduit's axis, depth, and width ($-L/2 \leqslant x \leqslant L/2$, $-H/2 \leqslant y \leqslant H/2$, and $-W/2 \leqslant z \leqslant W/2$). The width of the conduit is assumed to be much larger than its height ($W/H \gg 1$), and the flow is considered two dimensional (in the x-y plane). Figure 1 depicts schematically the conduit's cross section that lies in the x-y plane. We consider two different electrode arrangements. In the first case [Fig. 1(a)], a single pair of electrodes of length L_S are deposited along the conduit's walls ($-L_S/2 \leqslant x \leqslant L_S/2$, $y = \pm H/2$). The leading edge of the electrodes is located a distance L_1 downstream of the conduit's entrance. In the second arrangement [Fig. 1(b)], few shorter electrode pairs, each of length L_E, are positioned along the opposing walls. There is a dielectric gap S between adjacent electrode pairs, and the first electrode pair is located a distance L_1 downstream from the conduit's inlet ($x = -L/2$). The portions of the conduit's walls that are not coated with electrodes are dielectric. When we compare Figs. 1(a) and 1(b), the total length of the electrodes in Fig. 1(b) will be equal to the length of the electrodes in Fig. 1(a). There are two reasons to consider the case in Fig. 1(b). As we shall see, for equivalent total lengths of the electrodes, Fig. 1(b) offers an advantage as this configuration allows for higher current flow through the conduit than Fig. 1(a) does. Furthermore, the arrangement of Fig. 1(b) offers yet another

Downloaded 18 Oct 2007 to 158.130.69.60. Redistribution subject to AIP license or copyright, see http://pof.aip.org/pof/copyright.jsp

means of controlling the flow rate in the conduit. In Fig. 1(a), the flow rate is controlled by modifying the potential difference (or the current) across the electrode pair. In Fig. 1(b), the flow rate can also be controlled by adjusting the number of electrode pairs engaged. For example, one can apply either zero or a predetermined potential difference across any pair of electrodes in Fig. 1(b). As the number of engaged electrode pairs increases so does the flow rate.

The conduit is filled with a dilute RedOx electrolyte solution. The potential difference imposed across the opposing electrodes induces an electric current with density $\mathbf{J}\ (\mathrm{A/m^2}) = J_x\hat{\mathbf{e}}_x + J_y\hat{\mathbf{e}}_y + J_z\hat{\mathbf{e}}_z$. Hereafter, bold letters denote vectors. $\hat{\mathbf{e}}_x$, $\hat{\mathbf{e}}_y$, and $\hat{\mathbf{e}}_z$ are, respectively, unit vectors in the x, y, and z directions. J_x, J_y, and J_z are the components of the current flux in the x, y, and z directions, respectively. The device is placed in a uniform, magnetic field of intensity $\mathbf{B} = B\hat{\mathbf{e}}_z$ directed in the z direction. The current and the magnetic field interact to produce a Lorentz force of density $\mathbf{J} \times \mathbf{B} = J_y B\hat{\mathbf{e}}_x - J_x B\hat{\mathbf{e}}_y$. In addition to the MHD force, the flow may also be driven or opposed by an external pressure gradient.

A. The mathematical model for the fluid motion

The motion of the incompressible fluid induced by the combination of the external pressure gradient and the Lorentz force is described with the Navier–Stokes equations

$$\nabla \cdot \mathbf{u} = 0 \tag{1}$$

and

$$\rho \frac{D\mathbf{u}}{Dt} = \mathbf{J} \times \mathbf{B} - \nabla_p + \mu \nabla^2 \mathbf{u}. \tag{2}$$

In the above, $\mathbf{u} = u_x\hat{\mathbf{e}}_x + u_y\hat{\mathbf{e}}_y + u_z\hat{\mathbf{e}}_z$ is the fluid's velocity; u_x, u_y, and u_z are, respectively, the velocity components in the x, y, and z directions; t is time; p is the pressure; and ρ and μ are, respectively, the liquid's density and viscosity. The first term on the right-hand side of Eq. (2) represents the Lorentz force. The Lorentz force plays a similar role to that of the pressure gradient. We assume that the natural convection induced by the density variations due to electrochemical reactions on the surfaces of electrodes does not play a major role. In the above, since the magnetic Reynolds number is very small, we neglected the induced magnetic field.

No-slip boundary conditions are specified on the surfaces of all solid walls. The boundary conditions at the conduit's inlet and exit are

$$p(-L/2,y,z) = P_1, \tag{3a}$$

$$\hat{\mathbf{e}}_y \cdot \mathbf{u}(-L/2,y,z) = 0, \tag{3b}$$

$$p(L/2,y,z) = P_2, \tag{3c}$$

and

$$\hat{\mathbf{e}}_y \cdot \mathbf{u}(L/2,y,z) = 0. \tag{3d}$$

The external pressure gradient is $(P_1 - P_2)/L$.

B. The model for multiion mass transport

In order to maintain relatively high current fluxes and achieve high flow rates without bubble generation and electrode corrosion, dilute RedOx electrolyte solution, consisting of ions such as Fe^{3+}, Fe^{2+}, and Cl^-, is used. We assume that the RedOx electrolyte solution contains N dissolved ionic species ($k = 1,\ldots,N$). The model can account for the presence of a supporting electrolyte. The flux density of each dissolved species due to convection, diffusion, and migration is given by

$$\mathbf{N}_k = \mathbf{u}c_k - D_k \nabla c_k - z_k m_k F c_k(\nabla V + \mathbf{u} \times \mathbf{B}), \quad k = 1,\ldots,N. \tag{4}$$

In the above, c_k is the molar concentration, D_k is the diffusion coefficient, z_k is the charge, and m_k is the electrical mobility of the kth ionic species. F is Faraday's constant ($F = 96\,484.6$ C/mol), and V is the electric potential in the electrolyte solution. $\mathbf{u} \times \mathbf{B}$ is the induction term. Typically, in microfluidic systems $\|\mathbf{u}\| < 10^{-2}$ m/s, $\|\mathbf{B}\| < 1$ T, $\|\nabla V\| > 10^3$ V/m, $\|\mathbf{u} \times \mathbf{B}/\nabla V\| < 10^{-5}$, and the induction term can be neglected.

Using the Nernst–Einstein relation, the mobility of species k is expressed in terms of diffusion coefficient D_k, the universal gas constant R, and the absolute temperature T,

$$m_k = \frac{D_k}{RT}, \quad k = 1,\ldots,N. \tag{5}$$

The concentration of each species is governed by the Nernst–Planck equation[26]

$$\frac{\partial c_k}{\partial t} + \nabla \cdot \mathbf{N}_k = 0, \quad k = 1,\ldots,N. \tag{6}$$

We assume that there are no homogeneous reactions.

Equations (6) consist of $N+1$ unknown variables: the concentrations of the N dissolved species and the electric potential V. The electroneutrality condition provides the $(N+1)$th equation

$$\sum_{k=1}^{N} z_k c_k = 0. \tag{7}$$

In the above, we neglected the electrical double layer next to the electrodes since the height of the channel is much larger than the thickness of the electrical double layer.

The current flux $\mathbf{J}$ in the electrolyte solution due to convection, diffusion, and migration is given by

$$\mathbf{J} = -F\sum_{k=1}^{N} z_k \mathbf{N}_k. \tag{8}$$

The current $\mathbf{J}$ induces magnetic field $\mathbf{b}$, which according to Ampere's law satisfies the equation $\mu\mathbf{J} = \nabla \times (\mathbf{B} + \mathbf{b})$. To determine the significance of $\mathbf{b}$, we estimate its order of magnitude. $\|\mathbf{J}\| \sim \|\sigma \nabla V\| \sim (1\ \mathrm{S/m})(10^3\ \mathrm{V/m}) = 10^3\ \mathrm{A/m^2}$, the permeability $\mu \sim 10^{-6}$ T m/A, and $\mathbf{b} \sim 10^{-3}$ T, $\|\mathbf{b}/\mathbf{B}\| \sim 10^{-3}$. Thus, in most cases, the induced magnetic field $\mathbf{b}$ can be neglected.

Downloaded 18 Oct 2007 to 158.130.69.60. Redistribution subject to AIP license or copyright, see http://pof.aip.org/pof/copyright.jsp

The boundary condition for an inert species (no electrode reactions occur for that species) and for all species at insulated boundaries is

$$\mathbf{n}\cdot\mathbf{N}_k = 0, \tag{9a}$$

where $\mathbf{n}$ is the unit vector normal to the surface.

The concentrations of each species at the inlet cross section ($x=-L/2$) are given by

$$c_k(-L/2,y,z) = c_{k0}, \quad k=1,\ldots,N, \tag{9b}$$

and obey the electroneutrality condition $\Sigma_{k=1}^{N} z_k c_{k0}=0$.

Furthermore, far upstream of the electrodes, we assume insignificant electric field

$$\mathbf{n}\cdot\nabla V(-L/2,y,z) = 0. \tag{9c}$$

The transport of species at the exit cross section ($x=L/2$) is dominated by convection:

$$\mathbf{n}\cdot\mathbf{N}_k = \mathbf{n}\cdot(c_k,\mathbf{u}), \quad k=1,\ldots,N \tag{9d}$$

and

$$\mathbf{n}\cdot\nabla V(L/2,y,z) = 0. \tag{9e}$$

For the RedOx couple, oxidation and reduction reactions occur, respectively, at the surfaces of the anode and cathode:

$$\mathrm{Ox} + ne^- \Leftrightarrow \mathrm{Red}. \tag{10}$$

When the RedOx couple is $FeCl_3/FeCl_2$ electrolyte solution, Ox and Red in the above reaction correspond, respectively, to Fe^{3+} and Fe^{2+}, and $n=1$. The Bulter–Volmer equation describes the kinetics of the electrodes' reactions:[26]

$$\mathbf{n}\cdot\mathbf{N}_{\mathrm{Red}} = -\mathbf{n}\cdot\mathbf{N}_{\mathrm{Ox}} = k_a c_{\mathrm{Ox}} e^{(-\alpha nF/RT)\eta} - k_d c_{\mathrm{Red}} e^{[(1-\alpha)nF/RT]\eta}, \tag{11}$$

where c_{Ox} and c_{Red} are the concentrations of the active ions that are involved in the electrodes reactions (10) at the edge of the electric double layer; α is the charge transfer coefficient for the cathodic reaction, usually ranging from 0.0 to 1.0; n represents the number of electrons exchanged in the reaction; k_a and k_d are, respectively, the forward and backward rate constants; and

$$\eta = (U-V) - E_0 \tag{12}$$

is the overpotential difference. In the above, U is the imposed potential on the electrode, V is the potential of the electrolyte solution at the edge of the electric double layer next to the electrode, and E_0 is the equilibrium potential drop across the electric double layer.

Witness that the momentum and mass transport equations are strongly coupled. The flow field affects the mass transport due to convection that affects the current flux, which, in turn, affects the flow field.

C. Dimensionless form of the mathematical model

To examine the relative importance of the various processes, we recast the equations in a dimensionless form. To this end, we balance the Lorentz and viscous forces. H, C_0, D_0, $V_0=RT/(nF)$, $(FD_0C_0)/H$, $Q_0=(FD_0C_0BH)/\mu$, (FD_0C_0B), H/Q_0, and D_0C_0/H are, respectively, the length scale, the concentration scale, the diffusion coefficient scale, the potential scale, the current flux scale, the velocity scale, the pressure scale, the time scale, and the flux scale. C_0 is the bulk concentration of one of the RedOx couple (i.e., $FeCl_2$) at the inlet cross section [Eq. (9b)]. D_0 is the diffusion coefficient of one of the ion species (i.e., Fe^{2+}). The dimensionless form of the mathematical model is

$$\nabla\cdot\overline{\mathbf{u}} = 0, \tag{13a}$$

$$\mathrm{Re}\left(\frac{\partial}{\partial\overline{t}} + \overline{\mathbf{u}}\cdot\nabla\right)\overline{\mathbf{u}} = \overline{\mathbf{J}}\times\hat{\mathbf{e}}_z - \nabla\overline{p} + \nabla^2\overline{\mathbf{u}}, \tag{13b}$$

$$\mathrm{Pe}\frac{\partial\overline{c_k}}{\partial\overline{t}} + \nabla\cdot\overline{\mathbf{N}}_k = 0, \quad k=1,\ldots,N, \tag{13c}$$

and

$$\sum_{k=1}^{N} z_k\overline{c_k} = 0. \tag{13d}$$

In the above, the variables with over bars represent dimensionless quantities. $\mathrm{Re}=(\rho Q_0 H)/\mu$ is the Reynolds number and $\mathrm{Pe}=(Q_0H)/D_0$ is the Peclet number.

The dimensionless flux is

$$\overline{\mathbf{N}}_k = \mathrm{Pe}\,\overline{\mathbf{u}}\,\overline{c_k} - \overline{D_k}\nabla\overline{c_k} - z_k\overline{D_k}\,\overline{c_k}\nabla\overline{V}, \quad k=1,\ldots,N, \tag{14}$$

where $\overline{D_k}=D_k/D_0$. The dimensionless current flux is

$$\overline{\mathbf{J}} = -\sum_{k=1}^{N} z_k\overline{\mathbf{N}}_k. \tag{15}$$

At the inlet and exit,

$$\overline{p}(-\varepsilon_1,\overline{y,z}) = \overline{p}_1, \tag{16a}$$

$$\hat{\mathbf{e}}_y\cdot\overline{\mathbf{u}}(-\varepsilon_1,\overline{y,z}) = 0, \tag{16b}$$

$$\overline{p}(\varepsilon_1,\overline{y,z}) = \overline{p}_2, \tag{16c}$$

and

$$\hat{\mathbf{e}}_y\cdot\overline{\mathbf{u}}(\varepsilon_1,\overline{y,z}) = 0. \tag{16d}$$

In the above, $\varepsilon_1=L/(2H)$. The inert species at all surfaces and all species at insulated surfaces satisfy

$$\mathbf{n}\cdot\overline{\mathbf{N}}_k = 0. \tag{17a}$$

At the inlet ($\overline{x}=-\varepsilon_1$),

$$\overline{c_k}(-\varepsilon_1,\overline{y,z}) = \overline{c_{k0}} = c_{k0}/C_0, \quad k=1,\ldots,N \tag{17b}$$

and

$$\mathbf{n}\cdot\nabla\overline{V}(-\varepsilon_1,\overline{y,z}) = 0. \tag{17c}$$

At the exit ($\overline{x}=\varepsilon_1$),

$$\mathbf{n}\cdot\overline{\mathbf{N}}_k = \mathbf{n}\cdot(\mathrm{Pe}\,\overline{c_k}\overline{\mathbf{u}}), \quad k=1,\ldots,N \tag{17d}$$

and

Downloaded 18 Oct 2007 to 158.130.69.60. Redistribution subject to AIP license or copyright, see http://pof.aip.org/pof/copyright.jsp

$$\mathbf{n} \cdot \nabla \overline{V}(\varepsilon_1, \overline{y,z}) = 0. \tag{17e}$$

On the surfaces of the electrodes, the boundary conditions for the active ions that are involved in the electrode reaction (10) are

$$\mathbf{n} \cdot \overline{\mathbf{N}}_{\mathrm{Red}} = -\mathbf{n} \cdot \overline{\mathbf{N}}_{\mathrm{Ox}} = D_a(\overline{c}_{\mathrm{Ox}} e^{-\alpha\overline{\eta}} - K\overline{c}_{\mathrm{Red}} e^{(1-\alpha)\overline{\eta}}), \tag{17f}$$

where $D_a = k_a H / D_0$ is the Damköhler number representing the ratio between the diffusion and reaction time scales, $K = k_d / k_a$ is the ratio between the dissociation and association rate constants, and $\overline{\eta} = (\overline{U} - \overline{V}) - \overline{E}_0$.

III. SOLVER VALIDATION

To solve the strongly coupled system [Eqs. (13a)–(13d)], we used the finite element package FEMLAB (version 3.1, www.femlab.com). We employed nonuniform elements with a larger number of elements next to the electrodes' surfaces, where concentration boundary layers are expected to be present. To verify the code, we compared FEMLAB predictions with solutions available in the literature for special cases such as an electrochemical reactor with known flow field.

We simulated the parallel-plate electrochemical reactor (PPER) described in the work of Georgiadou.[27] The PPER geometry is similar to the configuration depicted in Fig. 1(a). The computational domain consists of an upstream region, a downstream region, and the region between two parallel electrodes positioned along the opposing walls [Fig. 1(a)]. In contrast to the MHD problem, in the PPER reactor, a parabolic flow field is specified. Our results are in excellent agreement with the finite difference results of Georgiadou.[27]

The good agreement of our computational results with previously published data obtained with a different computational technique as well as other comparisons with specialized solutions for the electrochemical problem (not shown here) give us confidence in our computational results. We also verified that for the conditions studied here, the numerical solutions are convergent, independent of the size of the elements, and satisfy the various conservation laws.

IV. MHD FLOW WITH REDOX SPECIES IN THE ABSENCE OF SUPPORTING ELECTROLYTE

In this section, we present a few numerical results of MHD flow in a two-dimensional conduit of the RedOx electrolyte $FeCl_3/FeCl_2$ in the absence of supporting electrolyte. The electrolyte solution contains the three ions Cl^-, Fe^{3+}, and Fe^{2+} with the respective charge numbers −1, 3, and 2. The diffusion coefficients of Cl^-, Fe^{3+}, and Fe^{2+} at room temperature are, respectively, 2.03×10^{-9} m^2/s, 6.04×10^{-10} m^2/s, and 7.19×10^{-10} m^2/s.[28] We selected $D_0 = D^{2+}_{\mathrm{Fe}} = 7.19 \times 10^{-10}$ m^2/s as the diffusion coefficient scale. For the reaction $Fe^{3+} + e^- \Leftrightarrow Fe^{2+}$, the reaction rate constant $k_a \approx 6.0 \times 10^{-6}$ m/s.[29] We were not able to find documented values for k_d and α. We assume that $\alpha \sim 0.5$ (symmetric energy barrier) and $k_d \sim k_a = 6.0 \times 10^{-6}$ m/s. When studying the *I-V* characteristics of a ferricyanide/ferrocyanide couple, Bortels *et al.*[30] obtained a good agreement between their theoretical predictions and experimental observations when assuming $k_d \sim k_a$. We will assume that this relationship is also true in our case. Since the electrolyte is dilute, the density and viscosity of the RedOx electrolyte are similar to those of water ($\rho \sim 1000$ kg/m^3 and $\mu \sim 10^{-3}$ Pa s). In all our computations, the inlet concentrations $C_0 = 0.1M$, the temperature $T = 298$ K, and the magnetic field intensity $B = 0.4$ T. This magnetic field can be generated with either a permanent magnet or an electromagnet. The inlet concentrations of $FeCl_3$ and $FeCl_2$ are taken to be equal. In the computations, we will neglect natural convection due to concentration gradients.

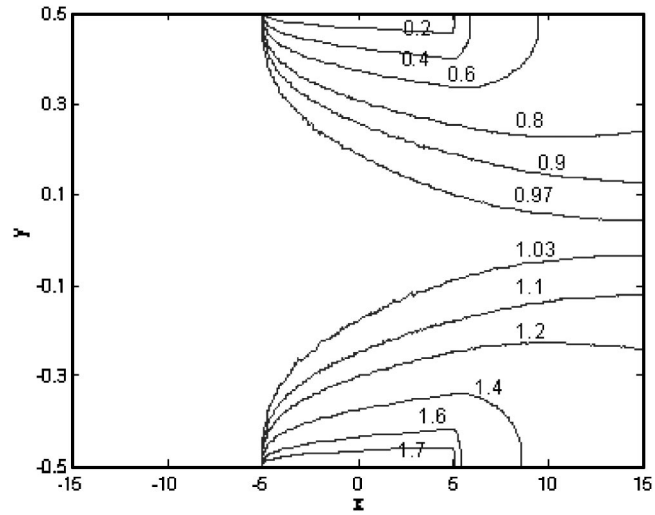

FIG. 2. The contours of the dimensionless concentration of the ion Fe^{3+} in a straight conduit with the electrode configuration depicted in Fig. 1(a). The imposed potentials on the surfaces of the anode ($y = -0.5$ and $-5 \leqslant x \leqslant 5$) and the cathode ($y = 0.5$ and $-5 \leqslant x \leqslant 5$) electrodes are, respectively, 0.5 V and −0.5 V. $\Delta\overline{p} = 0$, $C_0 = 0.1M$, $H = 1$ mm, $L_S/H = 10$, and $L/H = 30$.

All our computational results are given for a conduit with aspect ratio $L/H = 30$, total electrode length $L_S/H = 10$, and $H = 1$ mm. Computations were carried out for a conduit with a single electrode pair [the configuration depicted in Fig. 1(a)] and two electrode pairs [a configuration similar to the one depicted in Fig. 1(b)] both in the presence and absence of an external pressure difference $\overline{p}_1 - \overline{p}_2$. When the conduit is equipped with a single electrode pair [Fig. 1(a)], the anode is located at ($\overline{y} = -0.5$, $-5 \leqslant \overline{x} \leqslant 5$) and the cathode at ($\overline{y} = 0.5$, $-5 \leqslant \overline{x} \leqslant 5$). When the conduit is equipped with two electrode pairs [Fig. 1(b)], one electrode pair spans $-7.5 \leqslant \overline{x} \leqslant -2.5$ and the other electrode pair spans $2.5 \leqslant \overline{x} \leqslant 7.5$

Figures 2 and 3, respectively, depict the contours of the dimensionless concentration of the ions Fe^{3+} when the conduit is equipped with a single electrode pair [Fig. 1(a)] and when the conduit is equipped with two electrode pairs [Fig. 1(b)]. The imposed potentials at the anode and the cathode are, respectively, 0.5 V and −0.5 V, $\Delta p = 0$, $\mathrm{Re} \approx 2.8$, and $\mathrm{Pe} = 3860$. The contour lines for the concentrations of Fe^{2+} and Cl^- are similar to the ones depicted in Figs. 2 and 3 and, in the interest of space, are not reproduced here. In the upstream region [$-\varepsilon_1 \leqslant \overline{x} \leqslant -\varepsilon_2$, and $\varepsilon_2 = \varepsilon_1 - (L_1/H)$], the concentration of each ion is uniform and equal to the corresponding inlet concentration. In the interaction and the

Downloaded 18 Oct 2007 to 158.130.69.60. Redistribution subject to AIP license or copyright, see http://pof.aip.org/pof/copyright.jsp

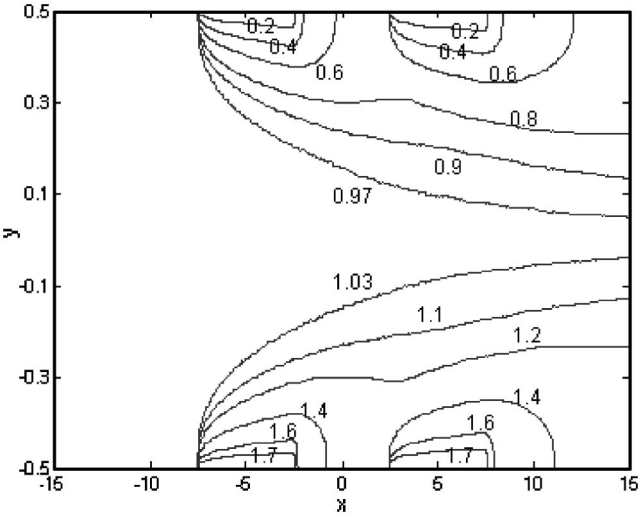

FIG. 3. The contours of the dimensionless concentration of the ion Fe^{3+} in a straight conduit equipped with two electrode pairs [Fig. 1(b)]. The imposed potentials on the surfaces of the anode ($y=-0.5$, $-7.5\leqslant x\leqslant -2.5$, and $2.5\leqslant x\leqslant 7.5$) and the cathode ($y=0.5$, $-7.5\leqslant x\leqslant -2.5$, and $2.5\leqslant x\leqslant 7.5$) electrodes are, respectively, 0.5 V and −0.5 V. $\Delta\overline{p}=0$, $C_0=0.1M$, $H=1$ mm, $L_E/H=5$, and $L/H=30$.

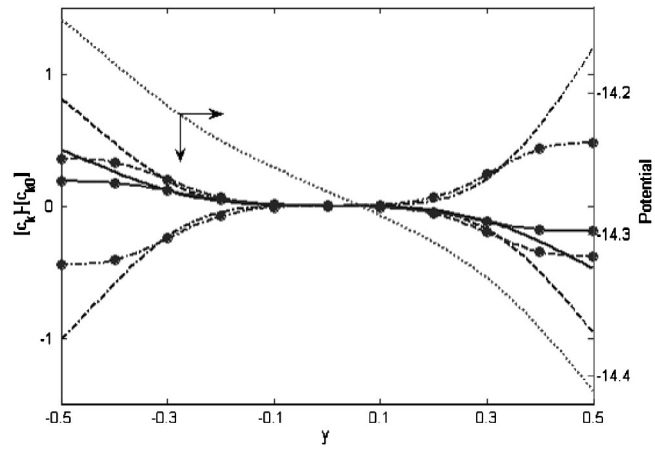

FIG. 4. The dimensionless concentration $[c_k(0,y)]-[c_{k0}]$ of the ions Cl^- (solid line), Fe^{3+} (dashed line), and Fe^{2+} (dash-dotted line), and the potential (dotted line) as functions of y. The lines without and with the symbols (•) correspond, respectively, to one pair [Fig. 1(a)] and two pairs [Fig. 1(b)] of electrodes. The imposed potentials on the surfaces of the anode ($y=-0.5$) and the cathode ($y=0.5$) electrodes are, respectively, 0.5 V and −0.5 V. $\Delta\overline{p}=0$, $C_0=0.1M$, $H=1$ mm, $L_E/H=10$, and $L/H=30$.

downstream regions ($-\varepsilon_2\leqslant\overline{x}\leqslant\varepsilon_1$), concentration boundary layers form next to both electrodes. The boundary layers arise from the electrochemical reactions on the electrodes' surfaces. On the surface of the cathode, the Fe^{3+} ion is consumed and the Fe^{2+} ion is produced through reduction. This leads to a lower concentration of the Fe^{3+} ion and a higher concentration of the Fe^{2+} ion next to the cathode. In order to maintain charge neutrality, the concentration of the Cl^- ion is reduced next to the surface of the cathode. On the surface of the anode, the ion Fe^{3+} is produced and the ion Fe^{2+} is consumed through the oxidation reaction, leading to a higher concentration of the ion Fe^{3+} and a lower concentration of the ion Fe^{2+}. Witness that when two electrode pairs are engaged, the thickness of the boundary layer is smaller than when only one electrode pair (with the same equivalent length) is engaged.

Figure 4 depicts the difference between the concentrations of the ions Fe^{2+} (dash-dotted line), Fe^{3+} (dashed line), and Cl^- (solid line) and their corresponding bulk concentrations and the potential (dotted line) as functions of y when $x=0$. The magnitude of the concentration and potential are specified, respectively, along the left and right axes of the figure. The conditions of Fig. 4 are the same as those of Figs. 2 and 3. The lines without and with the symbols (•) represent, respectively, the cases when one [Fig. 1(a)] and two [Fig. 1(b)] electrode pairs are engaged. There is no significant difference between the potential distributions in the case of the single and double electrode pairs. Away from the surfaces, in the core region, the concentration of each ion nearly equals its concentration at the conduit's inlet. Next to the electrode surfaces, boundary layers develop. Witness that the concentrations at the bottom (anode) and the top (cathode) surfaces are asymmetric $[c_k(\overline{x},-\overline{y})-\overline{c_{k0}}\neq -c_k(\overline{x},\overline{y})+\overline{c_{k0}}]$ with respect to the conduit's center. The asymmetry is due to both the nonlinear migration term in the expression for the flux (14) and the nonlinear Butler–Volmer boundary condition (17f).

Figure 5 depicts the vector field associated with the current flux at the electrodes' surfaces when a single electrode pair is engaged. The current flux is directed nearly normal to the electrodes' surfaces. As expected, the total amount of current leaving the anode equals the amount of current that goes through the cathode. The current flux depends strongly on the axial coordinate x and weakly on the transverse coordinate y.

Figure 6 depicts the y component of the current flux as a function of x along the conduit's axis ($y=0$) in the absence ($\Delta\overline{p}=0$, solid line) and the presence (dashed line) of an assisting external pressure difference ($\Delta\overline{p}=90$). In the electrodes' upstream and downstream regions, the current flux is zero. In the interaction (electrodes) region, the current flux

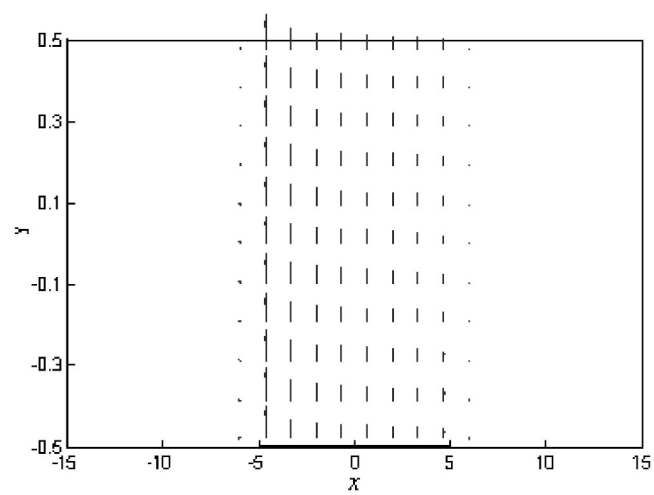

FIG. 5. The current flux field in a straight conduit. The imposed potentials on the surfaces of the anode ($y=-0.5$ and $-5\leqslant x\leqslant 5$) and the cathode ($y=0.5$ and $-5\leqslant x\leqslant 5$) electrodes are, respectively, 0.5 V and −0.5 V. $\Delta\overline{p}=0$, $C_0=0.1M$, $H=1$ mm, $L_S/H=10$, and $L/H=30$.

Downloaded 18 Oct 2007 to 158.130.69.60. Redistribution subject to AIP license or copyright, see http://pof.aip.org/pof/copyright.jsp

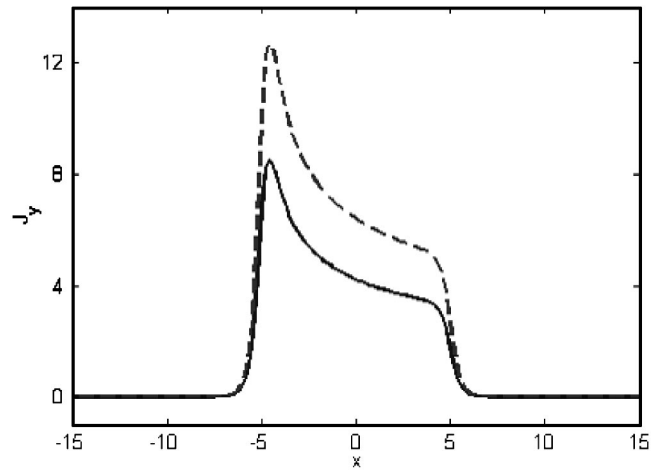

FIG. 6. The dimensionless y component of the current flux $\overline{J_y}(x,0)$ along the conduit's midplane as a function of x. The imposed potentials on the surfaces of the anode ($y=-0.5$ and $-5\leqslant x\leqslant 5$) and the cathode ($y=0.5$ and $-5\leqslant x\leqslant 5$) electrodes are, respectively, 0.5 V and −0.5 V. $C_0=0.1M$, $H=1$ mm, $L_E/H=10$, and $L/H=30$. The solid and dashed lines correspond, respectively, to the absence ($\Delta\overline{p}=0$) and presence ($\Delta\overline{p}=90$) of an external pressure difference.

decreases as x increases. The reduction in the current flux as x increases is due to the thickening of the concentration boundary layers. The thickness of the boundary layers increases as the electrodes' length increases, the Peclet number decreases, and the Damköhler number increases. As the assisting pressure difference increases, the induced flow increases, the thickness of the concentration boundary layer decreases, and the current flux increases.

The interaction between the y component of the current flux and the external magnetic field in the z direction produces the axial Lorentz (body) force that propels the liquid. Figure 7 depicts the axial velocity as a function of y at x

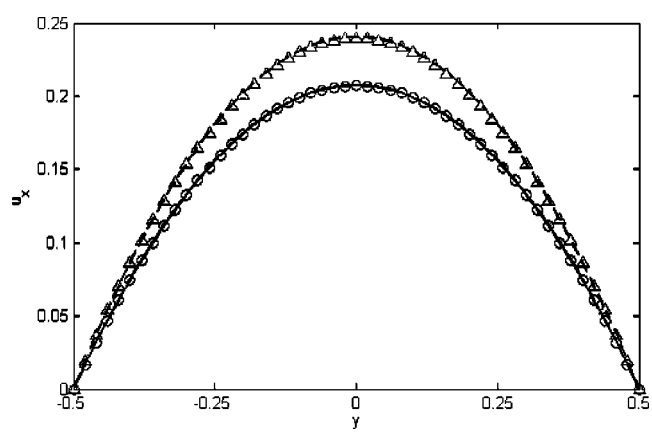

FIG. 7. The dimensionless x component of the velocity $u_x(0,y)$ as a function of y. The imposed potentials on the surfaces of the anode ($y=-0.5$) and the cathode ($y=0.5$) electrodes are, respectively, 0.5 V and −0.5 V. The solid line and the open circles (○) correspond to the case of one electrode pair ($-5\leqslant x\leqslant 5$, $y=\pm 0.5$). The dashed line and the open triangles (Δ) correspond to the case of two electrode pairs ($-7.5\leqslant x\leqslant -2.5$, $y=\pm 0.5$ and $2.5\leqslant x\leqslant 7.5$, $y=\pm 0.5$). The symbols and lines represent, respectively, the approximate formula (18) and the results of the numerical simulations. $\Delta\overline{p}=0$, $C_0=0.1M$, $H=1$ mm, the total length of the electrodes is $10H$, and $L/H=30$.

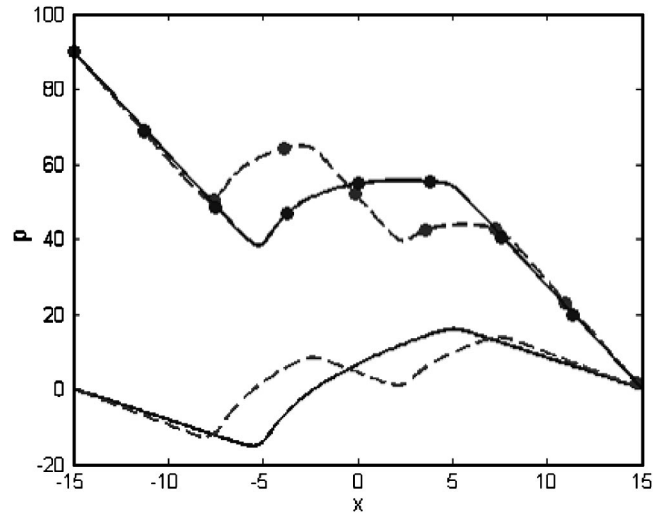

FIG. 8. The dimensionless pressure distribution $p(x,0)$ along the conduit's midplane as a function of x. The solid and dashed lines represent, respectively, the pressure distribution in the case of one electrode pair ($-5\leqslant x\leqslant 5$, $y=\pm 0.5$) and in the case of two electrode pairs ($-7.5\leqslant x\leqslant -2.5$, $y=\pm 0.5$ and $2.5\leqslant x\leqslant 7.5$, $y=\pm 0.5$). The lines without circles and with circles represent, respectively, $\Delta\overline{p}=0$ and $\Delta\overline{p}=90$. The imposed potentials on the surfaces of the anode ($y=-0.5$) and the cathode ($y=0.5$) electrodes are, respectively, 0.5 V and −0.5 V. $C_0=0.1M$, $H=1$ mm, the total length of the electrodes is $10H$, and $L/H=30$.

$=0$. The solid and dashed lines correspond, respectively, to a single pair of electrodes [Fig. 1(a)] and two pairs [Fig. 1(b)] of electrodes. In both the cases, there is no pressure difference between the conduit's inlet and exit. The velocity profile is nearly independent of the x coordinate, and it has the parabolic shape,

$$\overline{u(\overline{x},\overline{y})}=\frac{\overline{I}+(\overline{P_1}-\overline{P_2})}{8\overline{L}}(1-4\overline{y}^2), \tag{18}$$

where $\overline{I}$ is the dimensionless total electric current. Equation (18) represents a balance between the sum of the Lorentz and pressure forces and the viscous force in the momentum equation (13b), and it is derived by integrating the right-hand side (RHS) of the x-component momentum equation (13b) from $\overline{x}=-\overline{L}/2$ to $\overline{x}=\overline{L}/2$. The velocity profiles predicted by Eq. (18) for the cases of one and two electrode pairs are depicted, respectively, with the symbols (o) and (Δ) in Fig. 7. The approximations (symbols) are in a good agreement with the results of the numerical simulation (lines). The total current $\overline{I}$ (and the fluid flow rate) can be controlled, to a degree, by controlling the electrodes' potentials. When multiple electrode pairs are used, one can also control the current and the flow rate by engaging a desired number of electrodes. Although Eq. (18) appears simple, one must keep in mind that the current is not *a priori* known and it depends on the velocity.

Figure 8 depicts the dimensionless pressure along the conduit's axis as a function of x in the absence of an external pressure difference ($\Delta\overline{p}=0$, lines without symbols) and in the presence of an external pressure difference ($\Delta\overline{p}=90$, lines with solid circles). The solid and dashed lines correspond, respectively, to a single electrode pair [Fig. 1(a)] and two

Downloaded 18 Oct 2007 to 158.130.69.60. Redistribution subject to AIP license or copyright, see http://pof.aip.org/pof/copyright.jsp

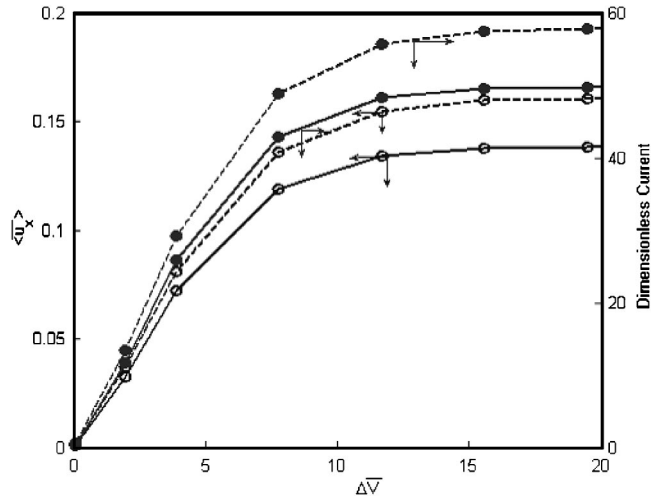

FIG. 9. The dimensionless total current (lines with solid symbols •) and cross-sectionally averaged dimensionless velocity $\langle u_x \rangle$ (lines with open symbols ○) are depicted as functions of the imposed dimensionless potential difference across the electrodes. The solid and dashed lines correspond, respectively, to a single pair [Fig. 1(a)] and two pairs [Fig. 1(b)] of electrodes. $\Delta\overline{p}=0$, $C_0=0.1M$, $H=1$ mm, the total length of the electrodes is $10H$, and $L/H=30$.

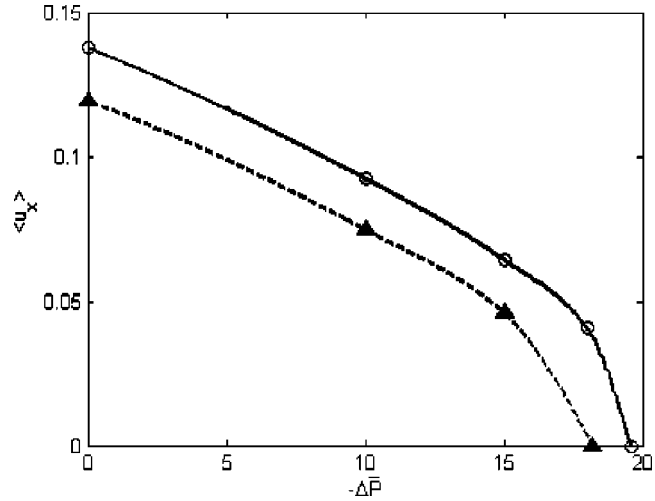

FIG. 10. The cross-sectionally averaged velocity $\langle u_x \rangle$ is depicted as a function of the adverse pressure difference when the potential differences $\Delta V=0.2$ V (dashed line with symbols ▲) and $\Delta V=0.4$ V (solid line with symbols ○) are applied across the electrodes in the case of a single electrode pair ($-5 \leqslant x \leqslant 5$, $y=\pm 0.5$). $C_0=0.1M$, $H=1$ mm, $L_E=10H$, and $L=30H$.

[Fig. 1(b)] electrode pairs with the same total length. The pressure is nearly uniform (independent of y) at any cross section. When only one pair of electrodes ($-5 \leqslant \overline{x} \leqslant 5$, $\overline{y}=\pm 0.5$) is engaged (solid lines), the pressure decreases nearly linearly in the upstream region, increases in the electrode region (the pumping region), and then decreases again nearly linearly in the downstream region. When two electrode pairs are engaged, the pressure decreases in the dielectric gap between the electrodes. Since the inlet and exit pressures are externally dictated, the pressure behavior far from the electrodes' locations is similar regardless of whether we have one or two electrode pairs. Recall, however, that when all else is equal, the flow rate in the case of two electrode pairs is higher than in the case of a single electrode pair (Fig. 7). The pressure $\overline{P}$ can be approximated with the equation

$$\overline{P}(\overline{x}) = \overline{P}_1 - \frac{(\overline{P}_1 - \overline{P}_2)}{\overline{L}}\overline{x} + \int_{-\varepsilon_2}^{\overline{x}} \overline{J}_y d\overline{x} - \frac{\overline{I}}{\overline{L}}\overline{x}. \tag{19}$$

In the upstream region, $\overline{J}_y=0$, the third term on the RHS of Eq. (19) equals zero, and $\overline{P}(\overline{x}) \approx \overline{P}_1 - \{[\overline{I}+(\overline{P}_1-\overline{P}_2)]/\overline{L}\}\overline{x}$. In the downstream region, $\int_0^{\overline{x}} \overline{J}_y(\xi,\overline{y})d\xi \approx \overline{I}$, and $\overline{P}(\overline{x}) \approx \overline{P}_1 + \overline{I} - \{[\overline{I}+(\overline{P}_1-\overline{P}_2)]/\overline{L}\}\overline{x}$.

Figure 9 depicts the flow rate $\langle \overline{u_x} \rangle = \int_{-1/2}^{1/2} \overline{u_x} d\overline{y}$ (lines with open circles) and the total electric current (lines with solid circles •) as functions of the imposed dimensionless potential difference $\Delta\overline{V}$ between the anode and the cathode when one pair (solid lines) and two pairs (dashed lines) of electrodes are positioned along the opposing walls and in the absence of an external pressure difference. The flow rate and current scales are given, respectively, along the left and right axes of the figure. When the applied potential difference is below a threshold value, both the current and flow rate increase as the potential difference increases. When the potential difference exceeds a certain critical value, both the current and flow rate reach their limiting values and become independent of the potential difference. When two pairs of electrodes are engaged, both the limiting current and the flow are higher than in the case when one electrode pair is engaged. Further increases in the potential difference will lead to undesired water electrolysis.

Next, we investigate the effect of adverse pressure difference on the flow rate. Figure 10 depicts the flow rate $\langle \overline{u_x} \rangle$ as a function of the adverse pressure difference when the potential differences $\Delta V=0.2$ V (dashed line with symbols ▲) and $\Delta V=0.4$ V (solid line with symbols o) are imposed across a single pair of electrodes. As the adverse pressure difference increases, the flow rate decreases until eventually the flow stalls (zero flow rate). When the adverse pressure difference is increased above the stall pressure, the flow will reverse direction. At low and moderate adverse pressure differences, the flow rate decreases nearly linearly as the adverse pressure difference increases. The rapid decline in the flow rate when the pressure difference approaches the stall pressure difference is due to the thickening of the concentration boundary layer and the reduction in the electric current $\overline{I}$. The flow rate can be expressed as

$$\langle \overline{u_x} \rangle \approx \frac{\overline{I}+(\overline{P}_1-\overline{P}_2)}{12\overline{L}}, \tag{20}$$

where the electric current $\overline{I}$ is a function of $\langle \overline{u_x} \rangle$. When the electric current $\overline{I}$ is directly controlled, the flow rate linearly decreases as the adverse pressure difference increases.

Figure 11 depicts the stall pressure difference as a function of the imposed potential difference across the electrodes when a single electrode pair is engaged. As the potential difference increases, the stall pressure difference increases until the limiting current has been reached. Once the limiting

Downloaded 18 Oct 2007 to 158.130.69.60. Redistribution subject to AIP license or copyright, see http://pof.aip.org/pof/copyright.jsp

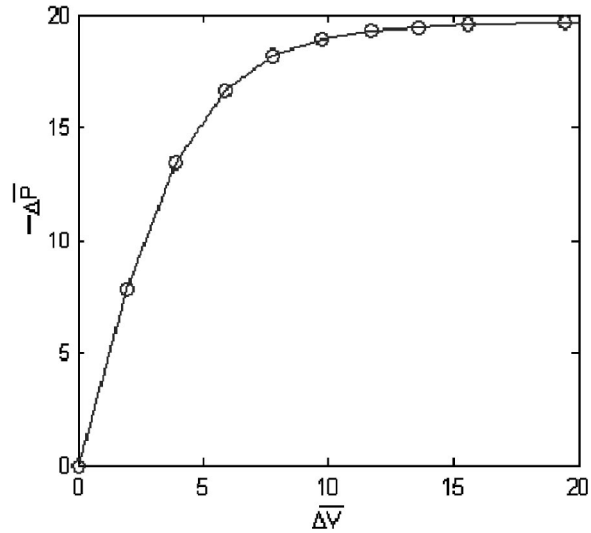

FIG. 11. The stall adverse pressure difference as a function of the imposed potential difference across the electrodes in the case of a single electrode pair ($-5 \leqslant x \leqslant 5$, $y=\pm 0.5$). $C_0=0.1M$, $H=1$ mm, $L_E=10H$, and $L=30H$.

current has been achieved, further increases in the potential difference do not contribute to increases in the stall pressure difference.

In this section, we studied the MHD flow in the conduit under conditions when diffusion and migration contributed nearly equally to the current flow. Under these circumstances, we were able to obtain relatively simple expressions for the velocity profile and pressure distributions as functions of the electric current. When the electrodes' potentials are controlled, the current depends on the velocity, and the simple expressions presented above are not sufficient to predict the velocity. In the following section, we develop an approximate analytical theory for the case when abundant supporting electrolyte is being used. The supporting electrolyte does not participate in the electrode reactions and its presence merely reduces the electric field in the electrolyte solutions.

V. MHD FLOW WITH REDOX SPECIES IN THE PRESENCE OF ABUNDANT SUPPORTING ELECTROLYTE AND UNDER LIMITING CURRENT CONDITIONS

The presence of abundant electrolyte allows us to neglect the migration term in the advection equation. Under steady state conditions, Eq. (13c) reduces to

$$\mathrm{Pe}^{-1}\left(\frac{\partial^2 \overline{c_k}}{\partial \overline{x}^2}+\frac{\partial^2 \overline{c_k}}{\partial \overline{y}^2}\right)=\frac{\overline{u_M}}{\overline{D_k}}(1-4\overline{y}^2)\frac{\partial \overline{c_k}}{\partial \overline{x}}, \quad k=1,\ldots,N. \tag{21}$$

In the above, we substituted the parabolic velocity profile [Eq. (18)], and $\overline{u_M}=\overline{I}+(\overline{P_1}-\overline{P_2})/8\overline{L}$ is the fluid's axial velocity at the conduit's center.

Typically, the diffusion coefficients are quite small and the Peclet numbers are large even when the velocities are moderate. Thus, we consider the limiting case of large Peclet numbers ($\mathrm{Pe}\to\infty$). We divide the flow domain into two regions: the core region away from the electrodes' surfaces and the concentration boundary layer regions next to the electrodes. To the first-order approximation, the concentration of each ion in the core region is equal to its concentration at the inlet (see Fig. 4):

$$\overline{c_k}=\overline{c_{k0}}+O(\mathrm{Pe}^{-1}). \tag{22}$$

In the boundary layer region, dominant balance suggests that $\partial^2\overline{c_k}/\partial\overline{y}^2 \sim O(\mathrm{Pe}^{2/3})$ and $\partial^2\overline{c_k}/\partial\overline{x}^2 \ll \partial^2\overline{c_k}/\partial\overline{y}^2$. It is convenient, therefore, to introduce the boundary layer variable η such that $\overline{y}=\mathrm{Pe}^{-1/3}\eta-\frac{1}{2}$. Accordingly, Eq. (21) becomes

$$\frac{\partial^2 \overline{c_{k\mathrm{BL}}}}{\partial \eta^2}=\frac{4\overline{u_M}}{\overline{D_k}}\eta(1-\mathrm{Pe}^{-1/3}\eta)\frac{\partial \overline{c_{k\mathrm{BL}}}}{\partial \overline{x}}, \tag{23}$$

where subscript BL denotes boundary layer variables. Formally, in the boundary layer, we introduce the asymptotic expansion

$$\overline{c_{k\mathrm{BL}}}=\overline{c_{k\mathrm{BL}}^{(0)}}+\mathrm{Pe}^{-1/3}\overline{c_{k\mathrm{BL}}^{(1)}}+O(\mathrm{Pe}^{-1/3}). \tag{24}$$

Substituting (24) into (23) and retaining only the leading order terms, we have

$$\frac{\partial^2 \overline{c_{k\mathrm{BL}}^{(0)}}}{\partial \tilde{\eta}_k^{\,2}}=\tilde{\eta}_k\frac{\partial \overline{c_{k\mathrm{BL}}^{(0)}}}{\partial \tilde{x}}. \tag{25}$$

In the above, for brevity, we introduced the variables with the wiggle superscript $\tilde{\eta}_k=(4\overline{u_M}/\overline{D_k})^{1/3}\eta$ and $\tilde{x}=\overline{x}+(L_S/2H)$. The concentration satisfies the asymptotic matching condition $\mathrm{im}_{\tilde{\eta}_k\to 0}\overline{c_{k\mathrm{BL}}^{(0)}}(\overline{x},\tilde{\eta}_k)=\overline{c_{k0}}$. Under limiting current conditions, the concentration of the Ox ion at the surface of the cathode and/or the Red ion at the surface of the anode equals zero. Hence,

$$\overline{c_{3\mathrm{BL}}^{(0)}}(\tilde{x},0)=0 \tag{26a}$$

and

$$\frac{\partial \overline{c_{2\mathrm{BL}}^{(0)}}(\tilde{x},0)}{\partial \tilde{\eta}_2}=-\left(\frac{\overline{D_3}}{\overline{D_2}}\right)^{2/3}\frac{\partial \overline{c_{3\mathrm{BL}}^{(0)}}(\tilde{x},0)}{\partial \tilde{\eta}_3}. \tag{26b}$$

In the above, $\overline{c_{2\mathrm{BL}}^{(0)}}$ and $\overline{c_{3\mathrm{BL}}^{(0)}}$ are, respectively, the concentrations of ions Fe^{3+} and Fe^{2+}. At the leading edge of the anode ($\tilde{x}=0$), the concentration of each ion is the same as the inlet concentration:

$$\overline{c_{k\mathrm{BL}}^{(0)}}(0,\tilde{\eta})=\overline{c_{k0}}, \quad k=2,3. \tag{27}$$

Next, we introduce the similarity variable (Lie group),

$$\tilde{\xi}_k=\tilde{x}^{-1/3}\tilde{\eta}_k, \quad k=2,3, \tag{28}$$

to reduce Eq. (25) to the ordinary differential equation

$$\frac{d^2 \overline{c_{k\mathrm{BL}}^{(0)}}}{d\tilde{\xi}_k^{\,2}}=-\frac{1}{3}\tilde{\xi}_k^{\,2}\frac{d\overline{c_{k\mathrm{BL}}^{(0)}}}{d\tilde{\xi}_k}, \quad k=2,3. \tag{29}$$

Integrating Eq. (29) twice yields

Downloaded 18 Oct 2007 to 158.130.69.60. Redistribution subject to AIP license or copyright, see http://pof.aip.org/pof/copyright.jsp

$$\overline{c}_{k\mathrm{BL}}^{(0)}(\tilde{\xi}_k) = A_k \int_0^{\tilde{\xi}_k} \exp\left(-\frac{\zeta^3}{9}\right) d\zeta + B_k, \quad k = 2,3, \tag{30}$$

where A_k and B_k are integration constants. Based on the boundary condition (26a), we have $B_3=0$. From the asymptotic matching and boundary condition (27), we have

$$A_3 = \frac{\overline{c}_{30}}{\int_0^\infty \exp(-\zeta^3/9) d\zeta} = \frac{3\Gamma(2/3)}{2(3)^{1/6}\pi}\overline{c}_{30} \approx 0.5384\overline{c}_{30}. \tag{31}$$

For the concentration $\overline{c}_{2\mathrm{BL}}^{(0)}$, based on the boundary condition (26b), we have

$$A_2 = -\left(\frac{\overline{D}_3}{\overline{D}_2}\right)^{2/3} A_3 \approx -0.5384\left(\frac{\overline{D}_3}{\overline{D}_2}\right)^{2/3} \overline{c}_{30}. \tag{32}$$

From the asymptotic matching with the core variable and boundary condition (27), we have

$$B_2 = \overline{c}_{20} + \left(\frac{\overline{D}_3}{\overline{D}_2}\right)^{2/3} \overline{c}_{30}. \tag{33}$$

Substituting the coefficients A_2, B_2, A_3 and B_3 into (30), we obtain the concentration distributions of the active ions in the boundary layer.

The dimensionless current density along the anode is

$$\overline{J}(\tilde{x}) = -(z_3 - z_2)\overline{D}_3 \mathrm{Pe}^{1/3} \frac{\partial \overline{c}_{3\mathrm{BL}}^{(0)}(\tilde{x},0)}{\partial \eta}. \tag{34}$$

Using (30), we have

$$\overline{J}(\tilde{x}) = -(z_3 - z_2)\overline{D}_3 \mathrm{Pe}^{1/3}\left(\frac{4\overline{u}_M}{\overline{D}_3}\right)^{1/3} A_3 \tilde{x}^{-1/3}. \tag{35}$$

In the above, $z_3=2$, $z_2=3$, $\overline{D}_3=1$, and $\overline{c}_{30}=1$. Hence Eq. (35) simplifies to

$$\overline{J}(\tilde{x}) = 0.8547\ \mathrm{Pe}^{1/3}\overline{u}_M^{1/3}\tilde{x}^{-1/3}. \tag{36}$$

Integrating (36) over $0 \leqslant \tilde{x} \leqslant L_s/H$, we have the total limiting current

$$\overline{I}_{\mathrm{lim}} = 1.282\ \mathrm{Pe}^{1/3}\overline{u}_M^{1/3}\left(\frac{L_s}{H}\right)^{2/3}. \tag{37}$$

Substituting $\overline{u}_M = [\overline{I} + (\overline{P}_1 - \overline{P}_2)]/8\overline{L}$, we have

$$8\overline{L}\overline{u}_M - (\overline{P}_1 - \overline{P}_2) = 1.282\ \mathrm{Pe}^{1/3}\overline{u}_M^{1/3}\left(\frac{L_s}{H}\right)^{2/3}. \tag{38}$$

In the absence of an external pressure difference,

$$\overline{u}_M = 0.0642\ \mathrm{Pe}^{1/2}\frac{L_s}{H}\left(\frac{1}{\overline{L}}\right)^{3/2}, \tag{39}$$

and the total limiting current is

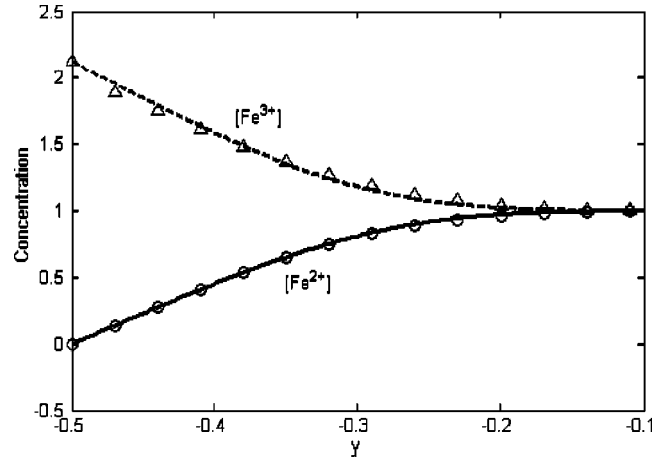

FIG. 12. The concentration distributions of the active ions Fe^{3+} (dashed line and Δ) and Fe^{2+} (solid line and o) as functions of y at cross section $x=0$ in the presence of abundant supporting electrolyte and under limiting current conditions in the case of a single electrode pair. The lines and symbols correspond, respectively, to the analytic boundary layer approximations and the numerical simulation.

$$\overline{I}_{\mathrm{lim}} = 0.5133\ \mathrm{Pe}^{1/2}\frac{L_s}{H}\left(\frac{1}{\overline{L}}\right)^{1/2}. \tag{40}$$

The dimensional limiting current is proportional to $B^{1/2}C_0^{3/2}$, which is consistent with the experimental observations of Aogaki *et al.*[24] for small conduits.

Based on (18) and (39), the induced MHD flow under limiting current conditions and in the absence of an external pressure difference can be approximated by

$$\overline{u(x,y)} = 0.0642\ \mathrm{Pe}^{1/2}\frac{L_s}{L}\left(\frac{H}{L}\right)^{1/2}(1 - 4\overline{y}^2). \tag{41}$$

Thus, the induced MHD flow is proportional to $Q_0^{3/2}$ and $(BC_0)^{3/2}$, which is also consistent with the experimental observations of Aogaki *et al.*[24] in small conduits.

Next, we compare the approximate analytical solutions with the results of numerical simulations. We simulate the presence of abundant supporting electrolyte by removing the migration term from the expression for the flux (14). In the case of a single electrode pair, in the presence of abundant supporting electrolyte, under limiting current conditions, and in the absence of an external pressure difference, Fig. 12 depicts the concentration of the active ions Fe^{3+} (dashed line and symbols Δ) and Fe^{2+} (solid line and symbols o) as functions of y at cross section $x=0$. The lines and symbols correspond, respectively, to the approximate analytical expressions (30) and the results of the numerical simulations. The analytical and numerical results are in excellent agreement. Figure 13 depicts the limiting current flux as a function of $\overline{x}$ along the anode under the same conditions as in Fig. 12. The solid line and the circles correspond, respectively, to the approximate analytical equation (36) and the results of the numerical simulation. Again the analytical and numerical results are in excellent agreement. The current flux attains its maximum value at the electrode's leading edge and decays as the distance from the leading edge increases. The induced

Downloaded 18 Oct 2007 to 158.130.69.60. Redistribution subject to AIP license or copyright, see http://pof.aip.org/pof/copyright.jsp

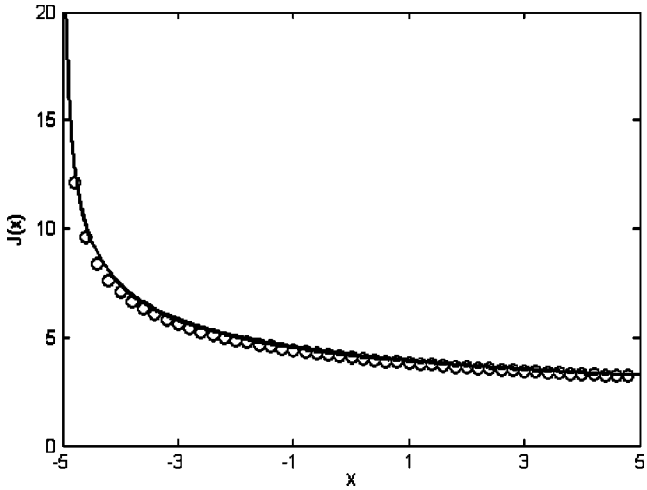

FIG. 13. The dimensionless limiting current flux as a function of x along the anode in the presence of abundant supporting electrolyte solution and under limiting current conditions in the case of a single electrode pair. The line and circles represent, respectively, the limiting current flux obtained with the analytic boundary layer approximation and the numerical simulation.

velocity profile obtained from the approximate analytic solution (41) is also in excellent agreement with the numerical results (not shown here).

VI. CONCLUSIONS

We solved the coupled problem for the ion concentration distribution and the flow field for magnetohydrodynamically driven flow in a straight conduit equipped with pairs of electrodes along its opposing walls. The concentration, current, and potential distributions and the flow fields were presented as functions of space coordinates. The calculations took into account the electrochemical reactions on the electrode surfaces and were carried out both in the presence and in the absence of external pressure differences.

Under conditions common in straight conduits, the velocity achieves a fully developed, parabolic profile at a relatively short distance from the conduit's inlet. In contrast, the concentration distributions exhibit boundary layer structures next to the electrodes' surfaces.

When the potential difference across the electrodes is below a certain threshold value, both the current and the flow rate increase as the potential difference increases. One can also control the flow rate by equipping the conduit with a large number of individually controlled electrode pairs and adjusting the number of the electrode pairs engaged. The selection of the various parameters such as the number of electrode pairs, the electrode pairs' length L_E, and the dielectric gap S that provide the highest flow rate is a design optimization problem that we do not address here.

In the presence of abundant supporting electrolyte and under limiting current conditions, we used boundary layer theory to derive approximate analytical expressions for the ion concentration distributions, the current flux, and the velocity of the induced MHD flow. The approximate analytical results are in excellent agreement with the results of numerical simulations. The limiting current and the induced flow rate are proportional to $B^{1/2}C_0^{3/2}$ and $(BC_0)^{3/2}$, respectively.

The results of the work are applicable to the design of MHD pumps that operate with RedOx electrolyte solutions. The use of a RedOx electrolyte solution such as $FeCl_3/FeCl_2$ facilitates a relatively high current flux at a low potential difference without electrode corrosion, electrolyte depletion, or bubble formation. Additionally, the work is relevant to various electrocatalytic and bioelectrocatalytic transformations and processes in which magnetic fields are applied to enhance mass transfer.

ACKNOWLEDGMENTS

The work described in this paper was supported, in part, by a NIH STTR Grant (Grant No. R41 RR018443-01) via Vegrandis, Inc. and by the DARPA SIMBIOSYS Program (Grant No. N66001-01-C-8056, Dr. Anantha Krishnan, program director). The authors are grateful to the FEMLAB support team, especially Dr. Peter Georén, for technical assistance.

[1] H. H. Woodson and J. R. Melcher, *Electromechanical Dynamics* (Wiley, New York, 1969), Vol. III.
[2] P. A. Davidson, *An Introduction to Magnetohydrodynamics* (Cambridge University Press, Cambridge, 2001).
[3] J. Jang and S. S. Lee, "Theoretical and experimental study of MHD (magnetohydrodynamic) micropump," Sens. Actuators, A **A80**, 84 (2000).
[4] A. V. Lemoff and A. P. Lee, "An AC magnetohydrodynamic micropump," Sens. Actuators B **63**, 178 (2000).
[5] H. H. Bau, "A case for magneto-hydrodynamics (MHD)," IMECE 2001, MEMS 23884 Symposium Proceedings, New York, November 2001 (unpublished).
[6] J. H. Zhong, M. Yi, and H. H. Bau, "Magneto hydrodynamic (MHD) pump fabricated with ceramic tapes," Sens. Actuators, A **A96**, 59 (2002).
[7] H. H. Bau, J. Zhong, and M. Yi, "A minute magneto hydro dynamic (MHD) mixer," Sens. Actuators B **79**, 205 (2001).
[8] H. H. Bau, J. Zhu, S. Qian, and Y. Xiang, "A magneto-hydrodynamic micro fluidic network," IMECE 2002-33559, Proceedings of IMECE'02, 2002 ASME International Mechanical Engineering Congress & Exposition, New Orleans, Louisiana, November 17–22 2002 (unpublished).
[9] H. H. Bau, J. Zhu, S. Qian, and Y. Xiang, "A magneto-hydrodynamically controlled fluidic network," Sens. Actuators B **88**, 207 (2003).
[10] J. West, J. P. Gleeson, J. Alderman, J. K. Collins, and H. Berney, "Structuring laminar flows using annular magnetohydrodynamic actuation," Sens. Actuators B **96**, 190 (2003).
[11] J. C. T. Eijkel, A. Van den Berg, and A. Manz, "Cyclic electrophoretic and chromatographic separation methods," Electrophoresis **25**, 243 (2004).
[12] J. West, B. Karamata, B. Lillis, J. P. Gleeson, J. Alderman, J. K. Collins, W. Lane, A. Mathewson, and H. Berney, "Application of magnetohydrodynamic actuation to continuous flow chemistry," Lab Chip **2**, 224 (2002).
[13] J. P. Gleeson, O. M. Roche, J. West, and A. Gelb, "Modeling annular micromixers," SIAM J. Appl. Math. **64**, 1294 (2004).
[14] G. Taylor, "Dispersion of a soluble matter in solvent flowing slowly through a tube," Proc. R. Soc. London, Ser. A **219**, 186 (1953).
[15] M. Yi, S. Qian, and H. H. Bau, "A magnetohydrodynamic chaotic stirrer," J. Fluid Mech. **468**, 153 (2002).
[16] S. Qian, J. Zhu, and H. H. Bau, "A stirrer for magnetohydrodynamically controlled minute fluidic networks," Phys. Fluids **14**, 3584 (2002).
[17] Y. Xiang and H. H. Bau, "Complex magnetohydrodynamic low-Reynolds-number flows," Phys. Rev. E **68**, 016312 (2003).
[18] S. Qian and H. H. Bau, "Magnetohydrodynamic stirrer for stationary and moving fluids," Sens. Actuators B **106**, 859 (2005).
[19] G. Hinds, F. E. Spada, J. M. D. Coey, T. R. N. Mhiochain, and M. E. G. Lyons, "Magnetic field effects on copper electrolysis," J. Phys. Chem. B **105**, 9487 (2001).
[20] T. Z. Fahidy, "Magnetoelectrolysis," J. Appl. Electrochem. **13**, 553 (1983).
[21] N. Leventis and X. R. Gao, "Magnetohydrodynamic electrochemistry in the field of Nd-Fe-B magnets. Theory, experiment, and application in self-powered flow delivery systems," Anal. Chem. **73**, 3981 (2001).

Downloaded 18 Oct 2007 to 158.130.69.60. Redistribution subject to AIP license or copyright, see http://pof.aip.org/pof/copyright.jsp

[22] A. Sugiyama, M. Hashiride, R. Morimoto, Y. Nagai, and R. Aogaki, "Application of vertical micro-disk MHD electrode to the analysis of heterogeneous magneto-convection," Electrochim. Acta **49**, 5115 (2004).
[23] O. Lioubashevski, E. Katz, and I. Willner, "Magnetic field effects on electrochemical processes: A theoretical hydrodynamic model," J. Phys. Chem. B **108**, 5778 (2004).
[24] R. Aogaki, K. Fueki, and T. Mukaibo, "Diffusion process in viscous-flow of electrolyte solution in magnetohydrodynamic pump electrodes," Denki Kagaku **44**, 89 (1976).
[25] G. B. N. Boum and A. Alemany, "Numerical simulations of electrochemical mass transfer in electromagnetically forced channel flows," Electrochim. Acta **44**, 1749 (1999).
[26] J. Newman, *Electrochemical Systems*, 2nd ed. (Prentice-Hall, Englewood Cliffs, NJ, 1991).
[27] M. Georgiadou, "Modeling current density distribution in electrochemical systems," Electrochim. Acta **48**, 4089 (2003).
[28] Y. Marcus, *Ion Properties* (Marcel Dekker, New York, 1997).
[29] M. D. Benari and G. T. Hefter, "Electrochemical characteristics of the Iron (III) Iron (II) system in dimethylsulfoxide solutions," Electrochim. Acta **36**, 471 (1991).
[30] L. Bortels, B. Van den Bossche, J. Deconinck, S. Vandeputte, and A. Hubin, "Analytical solution for the steady-state diffusion and migration involving multiple reacting ions: Application to the identification of Butler-Volmer kinetic parameters for the ferri-/ferrocyanide redox couple," J. Electroanal. Chem. **429**, 139 (1997).

Downloaded 18 Oct 2007 to 158.130.69.60. Redistribution subject to AIP license or copyright, see http://pof.aip.org/pof/copyright.jsp